ACS OMEGA

Open Access

http://pubs.acs.org/journal/acsodf

Article

Characterizing the Multiscale Knock Energy of the in-Cylinder Pressure of Compound Combustion Engines Fueled with Dimethyl Ether

Junxing Hou,* Wenshuai Hu, Zhenghe Wang, and Shuanghui Xi

Cite This: *ACS Omega* 2024, 9, 43406−43413

Read Online

ACCESS | Metrics & More | Article Recommendations

ABSTRACT: A two-cylinder, direct injection, and four-stroke naturally aspirated diesel engine is reformed to the compound combustion engine fueled with dimethyl ether. The wavelet energy spectra of the in-cylinder pressure with normal combustion and knocking combustion in a compound combustion engine are experimentally studied. The effects of the port fuel quantity, engine load, and engine speed on them are analyzed. The multiscale knock energy characteristics of the in-cylinder pressure are investigated based on wavelet energy and the Shannon entropy−energy ratio. The result shows that the in-cylinder pressure oscillation tends to be violent with the increase of port fuel quantity, the peak in-cylinder pressure increases, and its crank angle phase advances. With the increase in port fuel quantity, the wavelet energy of high-frequency detail signals d1, d2, and d3 obtained from wavelet decomposition all increases and the Shannon entropy−energy ratio decreases. The high-frequency detail signal d1 is more sensitive than the other detail signals. The frequency band of 5−10 kHz is the knock characteristic frequency band. The energy of the detail signal d1 increases significantly during knocking combustion, and the oscillation range enlarges and moves forward. The wavelet energy of detail signal d1 is the largest, and the Shannon entropy−energy ratio is the smallest at different brake mean effective pressures and different engine speeds. The effect of brake mean effective pressure and engine speed on the values is not obvious, and the port fuel quantity is the main factor.

1. INTRODUCTION

The energy crisis and environmental pollution are becoming increasingly severe, and it is urgent to implement the carbon neutrality strategy.[1,2] Developing low-carbon fuels and clean combustion technologies are the effective ways to solve the energy crisis and environmental pollution problems of vehicles at the present stage,[3−6] which is a relatively robust approach to implementing a carbon-neutral strategy and achieving sustainable development goals. Most vehicles were equipped with conventional direct injection (DI) engines. Homogeneous charge compression ignition (HCCI) combustion can use various fuels with few engine fuel system modifications. HCCI combustion has high thermal efficiency as well as reduced PM emissions and NO_x emissions.[7−10] However, knocking combustion occurs at high engine loads, and HCCI combustion cannot be controlled.[11−14] The HCCI−DI compound combustion is a clean combustion technology.[15−18] Dimethyl ether (DME) is considered a favorable carbon-neutral fuel and a renewable fuel. It has a high cetane number, good ignition quality, good renewability, and easy storage and transportation.[19−22] Currently, the studies of compound combustion engines fueled with DME have received increasing attention in research institutions at home and abroad, mainly focusing on compound combustion characteristics and emission control. The results show that compound combustion can extend the operating range with higher brake thermal efficiency and lower CO and HC emissions compared to HCCI combustion.[23,24] Effects of the DME premix ratio and exhaust gas recirculation (EGR) rate on the emission characteristics of DME-diesel premixed charge compression ignition (PCCI) combustion are investigated. The results show that NO_x emission reduced with an increase in the DME premix ratio and EGR rate, and smoke emission decreased with an increase in the DME premix ratio and a decrease in the EGR rate.[25] It is also observed that the effect of HCCI combustion on knocking combustion is always obvious. When the HCCI combustion proportion in the compound combustion is too large, knocking combustion occurs.[26−28]

Received: May 4, 2024
Revised: July 4, 2024
Accepted: July 26, 2024
Published: October 20, 2024

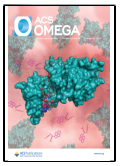

The wavelet energy spectra of the in-cylinder pressure at different scales in normal combustion and knocking combustion are experimentally studied in the paper. Based on the two indicators of wavelet energy and Shannon entropy−energy ratio, the effects of intake port fuel quantity, engine load, and engine speed on the multiscale energy characteristics of the in-cylinder pressure during normal combustion and knocking combustion were analyzed, revealing the energy characteristics at different scales. It is of great significance for identifying and controlling knocking combustion and optimizing combustion boundary parameters.

2. EXPERIMENTAL SETUP AND ANALYSIS METHOD

A two-cylinder, direct injection, and four-stroke naturally aspirated diesel engine is reformed into a DME compound combustion engine. The specifications of the base diesel engine are listed in Table 1. Figure 1 shows a schematic diagram of

Table 1. Specification of the Base Engine

bore × stroke (mm × mm)	135 × 145
compression ratio	16.5
rated power (kW)	29.4
rated speed (r/min)	1500
Nozzle orifice number × diameter (mm)	4 × 0.35
Nozzle opening pressure (MPa)	19
fuel delivery advance angle (°CA BTDC)	28

the DME compound engine test bench. As shown in Figure 1, in the DI combustion part of the compound combustion engine, DME in the fuel tank is filtered by a filter, pressurized by a low-pressure pump, pressurized by a high-pressure pump, and then injected into the engine cylinder. In the HCCI combustion part of the compound combustion engine, DME in the fuel tank is evaporated by an evaporator and mixed uniformly with air in the mixer on the intake duct and then enters the engine cylinder for HCCI combustion. In the compound combustion test, normal combustion and knocking combustion with different levels are achieved by adjusting the fuel amount of the HCCI combustion part. The in-cylinder pressure with normal combustion and knocking combustion during compound combustion is collected using the pressure sensor, the charge amplifier, and the data acquisition instrument.

Figure 2 is the schematic diagram of the discrete wavelet transform (DWT). The db5 wavelet function is selected for a three-layer discrete wavelet decomposition of the in-cylinder pressure. The in-cylinder pressure is decomposed into three high-frequency detail signals d1 (5−10 kHz), d2 (2.5−5 kHz),

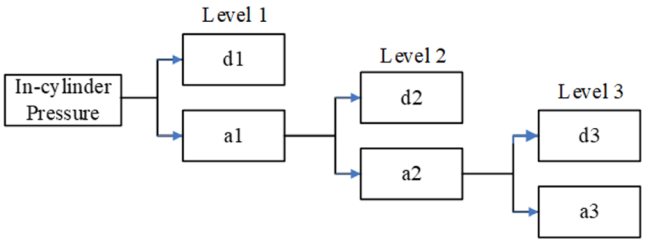

Figure 2. Principle of DWT.

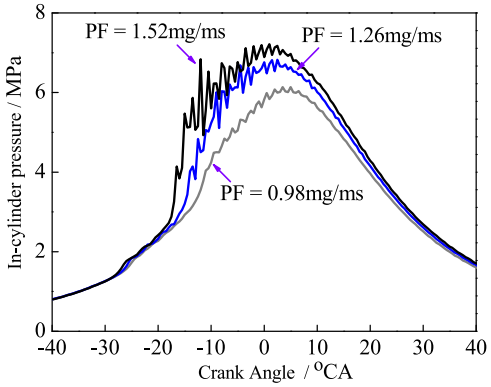

Figure 3. In-cylinder pressure for different PF values at 1500 rpm and 0.1 MPa BMEP.

and d3 (1.25−2.5 kHz) and one low-frequency smooth signal a3 (0−1.25 kHz). The signal a3 reflects the low-frequency information on the in-cylinder pressure, which is associated with less knocking combustion information, so it is not analyzed in the paper. The high-frequency detail signals d1, d2, and d3 reflect the local pressure oscillation information at different frequency domains, so they can reflect the knock energy characteristics at different scales.

The wavelet energy E_j and Shannon entropy−energy ratio HE are selected to evaluate the knock characteristics of the compound combustion in the paper. The more violent the knocking combustion is, the larger the wavelet energy value is and the smaller the Shannon entropy and the Shannon entropy−energy ratio is. The wavelet energy E_j, Shannon entropy H_{shan}, and Shannon entropy−energy ratio HE are defined as[29,30]

$$E_j = \sum_k |C_j(k)|^2 \tag{1}$$

$$H_{shan} = -\sum_k |C_j(k)|^2 \lg(|C_j(\bar{k})|)^2 \tag{2}$$

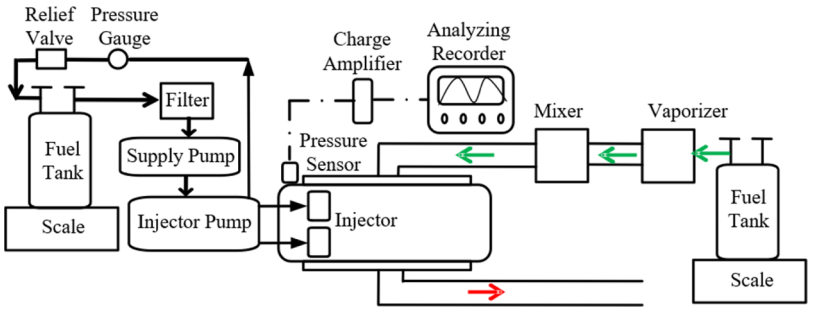

Figure 1. Schematic of a compound combustion test bench.

https://doi.org/10.1021/acsomega.4c04272
ACS Omega 2024, 9, 43406−43413

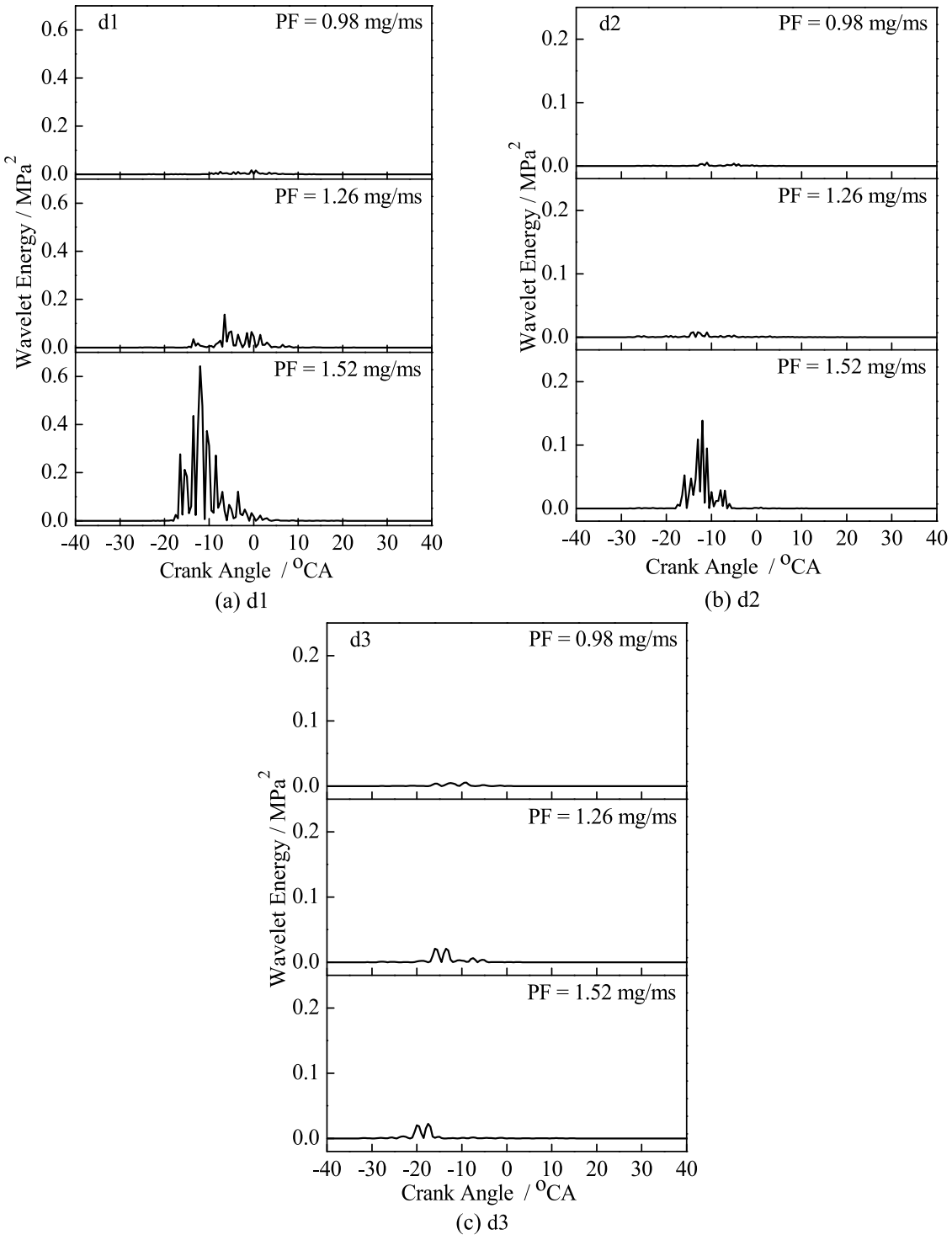

Figure 4. Wavelet energy spectrum for different PF values at 1500 r/min and 0.1 MPa BMEP.

$$HE=H_{shan}/E_j \quad (3)$$

$C_j(k)$ is the wavelet coefficient and j is the decomposition scale.

3. EXPERIMENTAL RESULTS AND ANALYSIS

3.1. Effect of Port Fuel on Multiscale Characteristics. The engine speed is 1500 rpm, and the brake mean effective pressure (BMEP) is 0.1 MPa. The port fuel (PF) amount of HCCI is 0.98, 1.26, and 1.52 mg/ms, respectively. Figure 3 shows the in-cylinder pressures for different PF values. It can be seen from Figure 3 that the irregularities in the in-cylinder pressure curve become larger as PF increases, indicating that the pressure oscillations become more severe, and the combustion becomes coarser. With the increase of PF, the accumulation of HCCI fuel quantity increases, knock intensity tends to increase, the peak in-cylinder pressure increases, and the phase of the crank angle, where the pressure peak occurs, advances. The pressure peaks/crank angle with three PF values

https://doi.org/10.1021/acsomega.4c04272
ACS Omega 2024, 9, 43406−43413

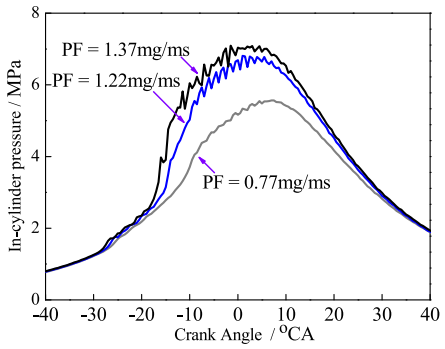

Figure 5. In-cylinder pressure for different PF values at 1500 rpm and 0.2 MPa BMEP.

are 6.14 MPa/3.5 °CA, 6.82 MPa/2.5 °CA, and 7.21 MPa/1 °CA, respectively.

The in-cylinder pressure is decomposed to the wavelet energy of the high-frequency detail signals d1, d2, and d3 at different scales by DWT. Figure 4 shows the wavelet energy spectrum of the in-cylinder pressure versus the crank angle for different PF values. For high-frequency detail signal d1 in Figure 4a, when the PF is 0.98 mg/ms, it can be seen clearly that the wavelet energy is basically zero during the combustion process, without any significant energy oscillations. When PF increases to 1.26 mg/ms, a series of small energy oscillations occur mainly between −9 and 2 °CA. When PF increases to 1.52 mg/ms, the energy oscillations increase sharply, and the ranges of the energy oscillations advance, mainly between −17 and 0 °CA. For high-frequency detail signal d2, when PF is

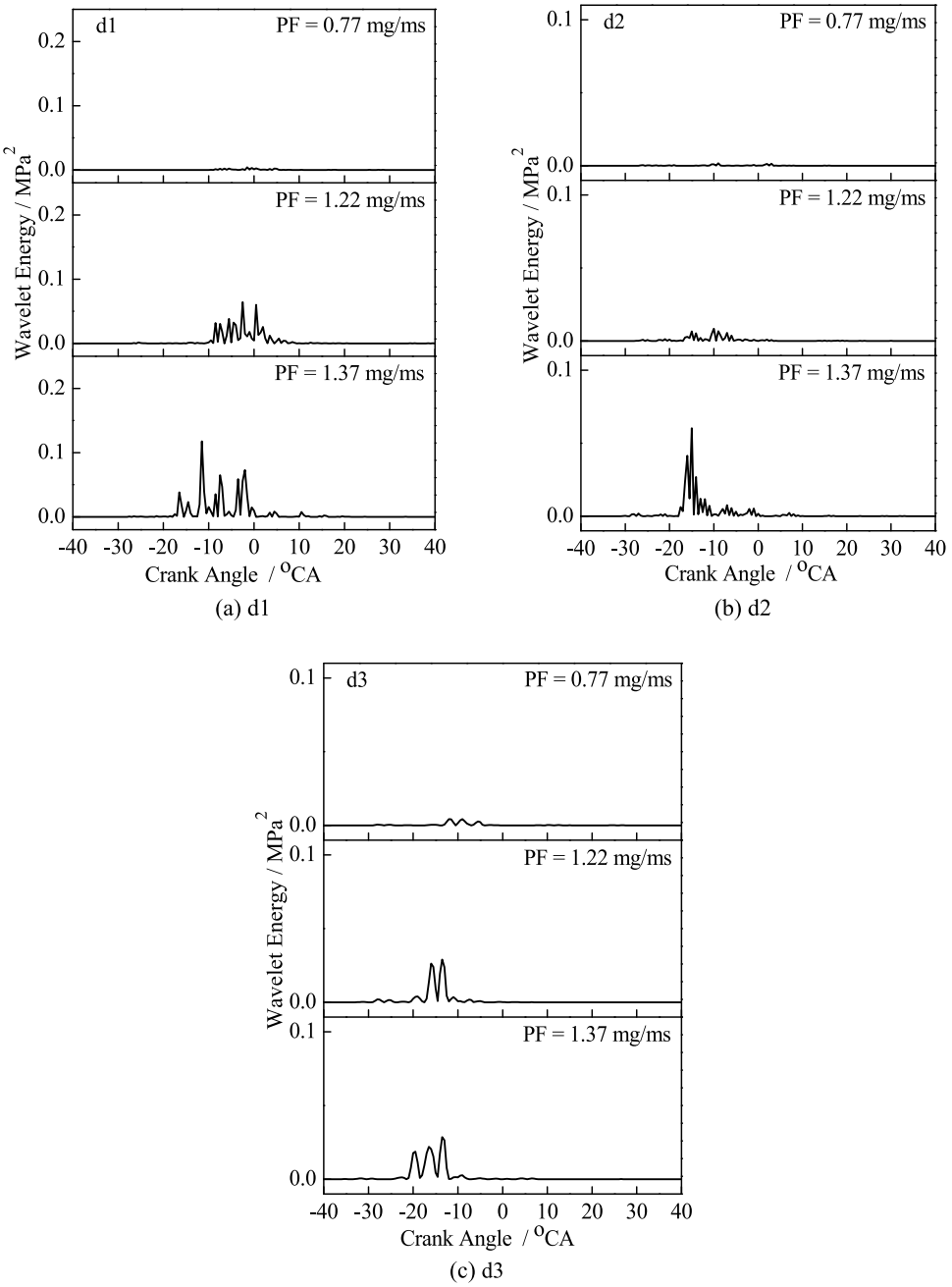

Figure 6. Wavelet energy for different PF values at 1500 rpm and 0.2 MPa BMEP.

https://doi.org/10.1021/acsomega.4c04272
ACS Omega 2024, 9, 43406−43413

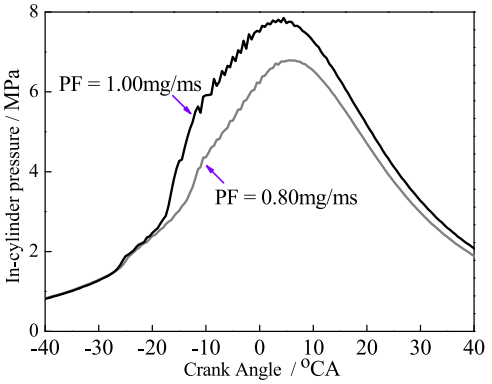

Figure 7. In-cylinder pressure for different PF values at 1100 r/min and 0.2 MPa BMEP.

0.98 and 1.26 mg/ms, the wavelet energy curve is almost a straight line, with small energy oscillations. When PF increases to 1.52 mg/ms, the energy oscillations increase significantly between −17 and −5.5 °CA, and the peak values of signal d2 are smaller than those of signal d1. For high-frequency detail signal d3 in Figure 4c, when PF is 0.98 mg/ms, the energy curve is basically a straight line; when PF increases to 1.26 and 1.52 mg/ms, double peaks appear in the energy oscillations, but the peaks are still small. As PF increases, the accumulation of HCCI fuel quantity increases, knock intensity tends to increase, and the range of energy oscillations advances. In summary, the combustion state changes from normal combustion to knocking combustion as PF increases, the in-cylinder pressure energy oscillations become more severe, the high-frequency detail signal d1 energy oscillations increase significantly, the oscillation range advances and expands, and the signal d1 is the most sensitive signal for knock energy. Its frequency band (5−10 kHz) is the knocking characteristic frequency band of the compound combustion engine, followed by signal d2 and signal d3.

3.2. Effect of Engine Load on Multiscale Characteristics. The engine speed keeps at 1500 r/min unchanged, and BMEP increases from 0.1 to 0.2 MPa. PF is 0.77, 1.22, and 1.37 mg/ms. Figure 5 shows the in-cylinder pressure at 1500 rpm and 0.2 MPa BMEP for different PF values. As shown in Figure 5, with the increase of PF, the accumulation of HCCI fuel quantity increases, knock intensity tends to increase, the peak in-cylinder pressure increases, the crank angle range of peak pressure advances, and the combustion becomes more violent. The peak in-cylinder pressure/crank angle for three PF values are 5.57 MPa/7 °CA, 6.81 MPa/1 °CA, and 7.09 MPa/−1.5 °CA, respectively.

Figure 6 shows the wavelet energy spectrum of the in-cylinder pressure at 1500 rpm and 0.2 MPa BMEP with different PF values. As can be seen from Figure 6, for the high-frequency detail signal d1, when PF is 0.77 mg/ms, the amplitude of the wavelet energy curve is very small. When PF increases to 1.22 mg/ms, a series of small energy oscillations appear between −9 and 3 °CA; and when PF further increases to 1.37 mg/ms, the energy oscillations increase and the

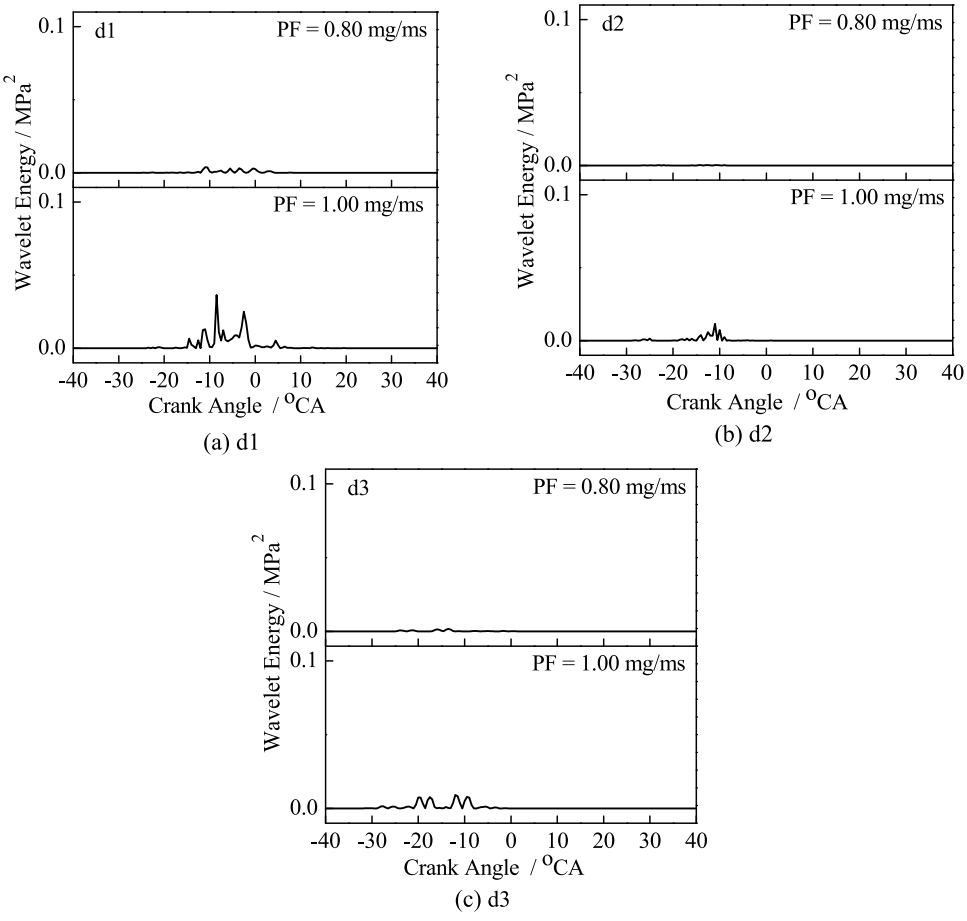

Figure 8. Wavelet energy for different PF values at 1100 rpm and 0.2 MPa BMEP.

https://doi.org/10.1021/acsomega.4c04272
ACS Omega 2024, 9, 43406−43413

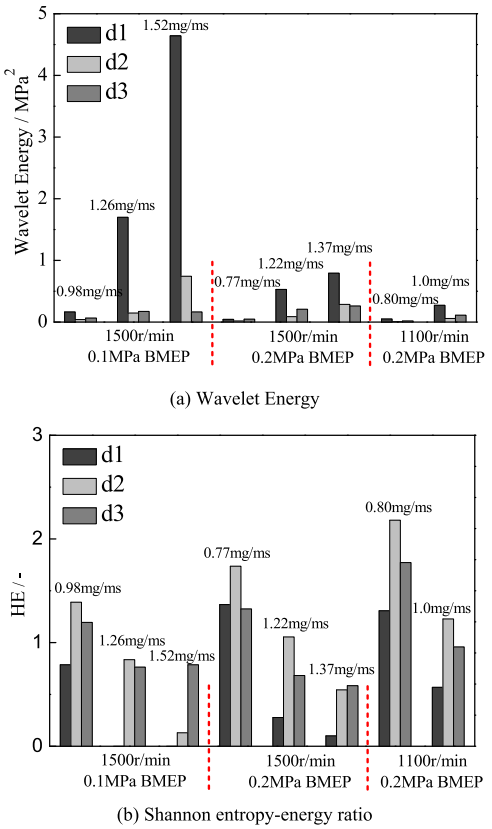

Figure 9. Wavelet energy and Shannon entropy−energy ratio for different PF values.

oscillation range moves forward between −17 and 0.5 °CA. For the high-frequency detail signal d2, when PF is 0.77 and 1.22 mg/ms, the energy curve is an almost straight line, and the peak oscillation energy is very small. When PF increases to 1.37 mg/ms, the energy oscillation increases significantly, and the oscillation range of the crank angle moves forward between −17 and −0.5 °CA. For the high-frequency detail signal d3, when PF is 0.77 mg/ms, the amplitude of the energy curve is small. When PF increases to 1.26 and 1.52 mg/ms, there are double oscillation peaks and triple oscillation peaks in the energy curves. With the increase of PF, the oscillation range moves forward and expands. It is between −17 and 12 °CA for 1.26 mg/ms and −21.5 and 12 °CA for 1.52 mg/ms. In summary, when BMEP increases from 0.1 to 0.2 MPa, the distributions of wavelet energy of the high-frequency detail signals d1, d2, and d3 remain unchanged. BMEP has no effect on them, with combustion status and knock intensity determining the distributions of multiscale wavelet energy of signals d1, d2, and d3.

3.3. Effect of Engine Speed on Multiscale Characteristics. BMEP remains at 0.2 MPa unchanged, and the engine speed adjusts from 1500 to 1100 r/min. Figure 7 shows the in-cylinder pressure at 1100 rpm and 0.2 MPa BMEP for different PF values. As shown in Figure 7, when PF is 0.80 mg/ms, the in-cylinder pressure curve is a smooth curve. The pressure peak is 6.79 MPa/5.5 °CA. As PF increases to 1.0 mg/ms, the peak in-cylinder pressure increases and the crank angle of the peak in-cylinder pressure advances. It is 7.85 MPa/4.5 °CA. HCCI combustion proportions in the compound combustion for two PF values are not too large; both of them are in normal combustion, and no obvious knocking combustion occurs.

Figure 8 shows the wavelet energy spectrum of the in-cylinder pressure at 1100 rpm and 0.2 MPa BMEP with different PF values. It can be seen from Figure 8 that when PF is 0.80 mg/ms, there are no obvious oscillations in the wavelet energy curves for high-frequency detail signals d1, d2, and d3. When PF increases to 1.00 mg/ms, energy oscillations occur in high-frequency detail signals d1, d2, and d3, the oscillation amplitude of the wavelet energy curve becomes larger, but the energy oscillations of signal d1 is sensitive and increases significantly with the maximum energy oscillation peak and the oscillation crank angle range of −15.5 to −1 °CA. In summary, the oscillation energy of signal d1 is the largest, and engine speed has no effect on it, while combustion status and knock intensity play a decisive role. It determines the distributions of multiscale wavelet energy of signals d1, d2, and d3.

Figure 9 shows the wavelet energy and Shannon entropy−energy ratio with different PF values. The largest wavelet energy and the smallest Shannon entropy−energy ratio reflect the knock energy law. As can be seen in Figure 9, the wavelet energy of signal d1 is the largest, and its Shannon entropy−energy ratio is the smallest at different BMEP and engine speeds. Therefore, signal d1 is the sensitive signal of knock energy and engine speed and BMEP has no effect on the knock energy value, while combustion status and knock intensity determine the knock energy value and Shannon entropy−energy ratio. As PF increases, the wavelet energy of signals d1, d2, and d3 gradually increases, the Shannon entropy−energy ratio gradually decreases, and the most sensitive signal is signal d1. The frequency band of 5−10 kHz is the knock characteristic frequency band.

4. CONCLUSIONS

The knock energy characteristics of the in-cylinder pressure in DME compound combustion are calculated using the novelty methods in the paper. Wavelet energy and Shannon entropy−energy ratio are introduced to evaluate the multiscale knock energy characteristics. The multiscale wavelet energy and multiscale Shannon entropy−energy ratio in normal combustion and knocking combustion are analyzed. The effects of port fuel quantity PF, engine load, and engine speed on the multiscale knock energy characteristics are revealed. The knock characteristic frequency band is determined. The results are listed as follows:

(1) With the increase of PF, the accumulation of HCCI fuel quantity increases, compound combustion tends to be violent, knock intensity and the pressure oscillation increase, the peak pressure increases, and its phase angle advances.

(2) The most sensitive signal to knock is signal d1, followed by signal d2 and signal d3. With the increase of PF, the combustion status changes from normal combustion to knocking combustion, the energy oscillation of signal d1 increases significantly, and the oscillation range moves forward and expands. The frequency band of 5−10 kHz of signal d1 is the knock characteristic frequency band.

(3) The wavelet energy of signal d1 is the largest, and the Shannon entropy−energy ratio is the smallest at different BMEP and different engine speeds. The effects of BMEP and engine speed are not obvious, while combustion status and knock intensity play a decisive role. With the increase of PF, the wavelet energy of signals d1, d2, and d3 gradually increases, while the

https://doi.org/10.1021/acsomega.4c04272
ACS Omega 2024, 9, 43406−43413

Shannon entropy−energy ratio gradually decreases, especially that of the sensitive signal d1.

AUTHOR INFORMATION

Corresponding Author

Junxing Hou − *School of Aerospace Engineering, Zhengzhou University of Aeronautics, 450046 Zhengzhou, China;* orcid.org/0000-0002-7903-6692; Email: houjunxing@126.com

Authors

Wenshuai Hu − *School of Aerospace Engineering, Zhengzhou University of Aeronautics, 450046 Zhengzhou, China*

Zhenghe Wang − *School of Mechanical Engineering, Zhengzhou University of Aeronautics, 450046 Zhengzhou, China*

Shuanghui Xi − *School of Mechanical Engineering, Zhengzhou University of Aeronautics, 450046 Zhengzhou, China;* orcid.org/0000-0002-1699-464X

Complete contact information is available at: https://pubs.acs.org/10.1021/acsomega.4c04272

Notes

The authors declare no competing financial interest.

ACKNOWLEDGMENTS

This work is supported by the Key Project of the Education Department of Henan Province (22A470010), the Science and Technology Plan Project of Henan Province (222102320329), and the Opening Fund of Henan Key Laboratory of General Aviation Technology (ZHKF-240211).

REFERENCES

(1) Zhao, X.; Ma, X.; Chen, B.; et al. Challenges toward carbon neutrality in China: Strategies and countermeasures. *Resour., Conserv. Recycl.* **2022**, *176*, No. 105959.

(2) Chen, L.; Msigwa, G.; Yang, M.; et al. Strategies to achieve a carbon neutral society: a review. *Environ. Chem. Lett.* **2022**, *20* (4), 2277−2310.

(3) Cardoso, J. S.; Silva, V.; Rocha, R. C.; et al. Ammonia as an energy vector: Current and future prospects for low-carbon fuel applications in internal combustion engines. *J. Cleaner Prod.* **2021**, *296*, No. 126562.

(4) García, A.; Monsalve-Serrano, J.; Villalta, D.; Guzmán-Mendoza, M. Optimization of low carbon fuels operation on a CI engine under a simplified driving cycle for transportation de-fossilization. *Fuel* **2022**, *310*, No. 122338.

(5) Kim, S.; Okada, S.; Matsuo, T.; et al. A new concept for high efficiency and clean diesel combustion by controlling mixture distribution with dual zone combustion chamber. *Int. J. Engine Res.* **2023**, *24* (10), 4421−4432.

(6) Shim, E.; Park, H.; Bae, C. Comparisons of advanced combustion technologies (HCCI, PCCI, and dual-fuel PCCI) on engine performance and emission characteristics in a heavy-duty diesel engine. *Fuel* **2020**, *262*, No. 116436.

(7) Yu, X.; LeBlanc, S.; Sandhu, N.; et al. Combustion control of DME HCCI using charge dilution and spark assistance. *Proc. Inst. Mech. Eng., Part D* **2023**, *237* (8), 1959−1974.

(8) Niklawy, W.; Shahin, M.; Amin, M. I.; Elmaihy, A. Comprehensive analysis of combustion phasing of multi-injection HCCI diesel engine at different speeds and loads. *Fuel* **2022**, *314*, No. 123083.

(9) Kocakulak, T.; Babagiray, M.; Nacak, Ç.; et al. Multi objective optimization of HCCI combustion fuelled with fusel oil and n-heptane blends. *Renewable Energy* **2022**, *182*, 827−841.

(10) Verma, S. K.; Gaur, S.; Akram, T.; et al. Emissions from homogeneous charge compression ignition (HCCI) engine using different fuels: a review. *Environ. Sci. Pollut. Res.* **2022**, *29* (34), 50960−50969.

(11) Khandal, S. V.; Banapurmath, N. R.; Gaitonde, V. N. Performance studies on homogeneous charge compression ignition (HCCI) engine powered with alternative fuels. *Renewable Energy* **2019**, *132*, 683−693.

(12) Miao, X.; Li, L.; Wang, S.; et al. Prediction and control of knock at high load boundary for HCCI engine based on neural network. *Fuel* **2023**, *333*, No. 126421.

(13) Gharehghani, A. Load limits of an HCCI engine fueled with natural gas, ethanol, and methanol. *Fuel* **2019**, *239*, 1001−1014.

(14) Li, G.; Zhang, C.; Zhou, J. Study on the knock tendency and cyclical variations of a HCCI engine fueled with n-butanol/n-heptane blends. *Energy Convers. Manage.* **2017**, *133*, 548−557.

(15) Fathi, M.; Jahanian, O. Fuel reactivity as a means to control DI-HCCI combustion engine. *J. Engine Res.* **2017**, *47* (47), 39−46.

(16) Roslan, M. F.; Veza, I.; Said, M. F. M. Effects of injection parameters and intake air temperature on acetone-butanol-ethanol (ABE) blend HCCI-DI engine. *Fuel* **2023**, *345*, No. 128250.

(17) Shi, L.; Ji, C.; Wang, S.; et al. Combustion and emissions characteristics of a SI engine fueled with gasoline-DME blends under different spark timings. *Fuel* **2018**, *211*, 11−17.

(18) Elkelawy, M.; Bastawissi, H. A. E.; El Shenawy, E. A.; et al. Influence of lean premixed ratio of PCCI-DI engine fueled by diesel/biodiesel blends on combustion, performance, and emission attributes; a comparison study. *Energy Convers. Manage.: X* **2021**, *10*, No. 100066.

(19) Thomas, G.; Feng, B.; Veeraragavan, A.; et al. Emissions from DME combustion in diesel engines and their implications on meeting future emission norms: A review. *Fuel Process. Technol.* **2014**, *119*, 286−304.

(20) Meng, X.; Zhang, M.; Zhao, C.; et al. Study of combustion and NO chemical reaction mechanism in ammonia blended with DME. *Fuel* **2022**, *319*, No. 123832.

(21) Benajes, J.; Novella, R.; Pastor, J. M.; et al. Computational optimization of the combustion system of a heavy-duty direct injection diesel engine operating with dimethyl-ether. *Fuel* **2018**, *218*, 127−139.

(22) Bae, C.; Kim, J. Alternative fuels for internal combustion engines. *Proc. Combust. Inst.* **2017**, *36* (3), 3389−3413.

(23) Ying, W.; Li, H.; Jie, Z.; Longbao, Z. Study of HCCI-DI combustion and emissions in a DME engine. *Fuel* **2009**, *88* (11), 2255−2261.

(24) Fang, Q.; Fang, J.; Zhuang, J.; Huang, Z. Influences of pilot injection and exhaust gas recirculation (EGR) on combustion and emissions in a HCCI-DI combustion engine. *Appl. Therm. Eng.* **2012**, *48*, 97−104.

(25) Zhao, Y.; Wang, Y.; Li, D.; et al. Combustion and emission characteristics of a DME (dimethyl ether)-diesel dual fuel premixed charge compression ignition engine with EGR (exhaust gas recirculation). *Energy* **2014**, *72*, 608−617.

(26) Hou, J.; Liu, J.; Wei, Y.; Jiang, Z. Experimental study on in-cylinder pressure oscillations of homogenous charge compression ignition−direct injection combustion engine fueled with dimethyl ether. *J. Energy Resour. Technol.* **2016**, *138* (5), No. 052211.

(27) Wang, Y.; Guo, C.; Wang, P.; Wang, D. Numerical investigation on knock combustion in a diesel−dimethyl ether dual-fuel engine. *Energy Fuels* **2019**, *33* (6), 5710−5718.

(28) Hou, J.; Wen, Z.; Liu, J.; Jiang, Z. Study on knock characteristics of dimethyl ether fueled homogenous charge compression ignition-direct injection combustion engines. *J. Energy Resour. Technol.* **2015**, *137* (6), No. 062202.

(29) Yan, X.; Dong, S.; Xu, B. Flaw diagnosis technology for remanufactured motor rotor based on optimal wavelet packet Shannon entropy. *J. Mech. Eng.* **2016**, *52* (4), 7−12.

(30) Hou, J.; Qiao, X.; Wang, Z.; et al. Characterization of knocking combustion in HCCI DME engine using wavelet packet transform. *Appl. Energy* **2010**, *87* (4), 1239−1246.

https://doi.org/10.1021/acsomega.4c04272
ACS Omega 2024, 9, 43406−43413